Supplementary Information

Effect of Fullerene on Anisotropy, Domain Size and Relaxation in a Perpendicularly Magnetized Pt/Co/C_{60}/Pt System

Purbasha Sharangi,[†] Aritra Mukhopadhyaya,[‡] Srijani Mallik,[†] Esita Pandey,[†] Brindaban Ojha,[†] Md. Ehesan Ali,[*,‡] and Subhankar Bedanta[*,†]

[†]*Laboratory for Nanomagnetism and Magnetic Materials (LNMM), School of Physical Sciences, National Institute of Science Education and Research (NISER), An OCC of Homi Bhabha National Institute (HBNI), Jatni 752050, Odisha, India*

[‡]*Institute of Nano Science and Technology, Knowledge City, Sector-81, Mohali, Punjab 140306, India*

E-mail: ehesan.ali@inst.ac.in; sbedanta@niser.ac.in

Structural information:

To understand the quality of interfaces we have performed X-ray reflectivity measurements using X-ray diffractometer (XRD) manufactured by Rigaku. Exact thickness and roughness of the samples have been determined by fitting the XRR data using GenX software. Figure S1 (a-d) show the XRR data and fitting for samples A1 to A4, respectively considering without any interdiffusion. The extracted thickness (t) and roughness (σ) of the layers are listed in Table S1. For thinner C_{60} samples (samples A2 and A3) the C_{60} layer may not be continuous. Therefore, we have fitted the XRR data considering Pt-C_{60} interdiffusion

(Figure S2 and Table S2). The XRR fits to the data yields roughness values comparable to the thickness of C_{60} layer, which indicates that the C_{60} layer may not be continuous in samples A2 and A3. Future cross-sectional transmission electron microscopy (TEM) may elucidate the nature of interface. The effect of interdiffusion on the magnetic properties to be understood in future.

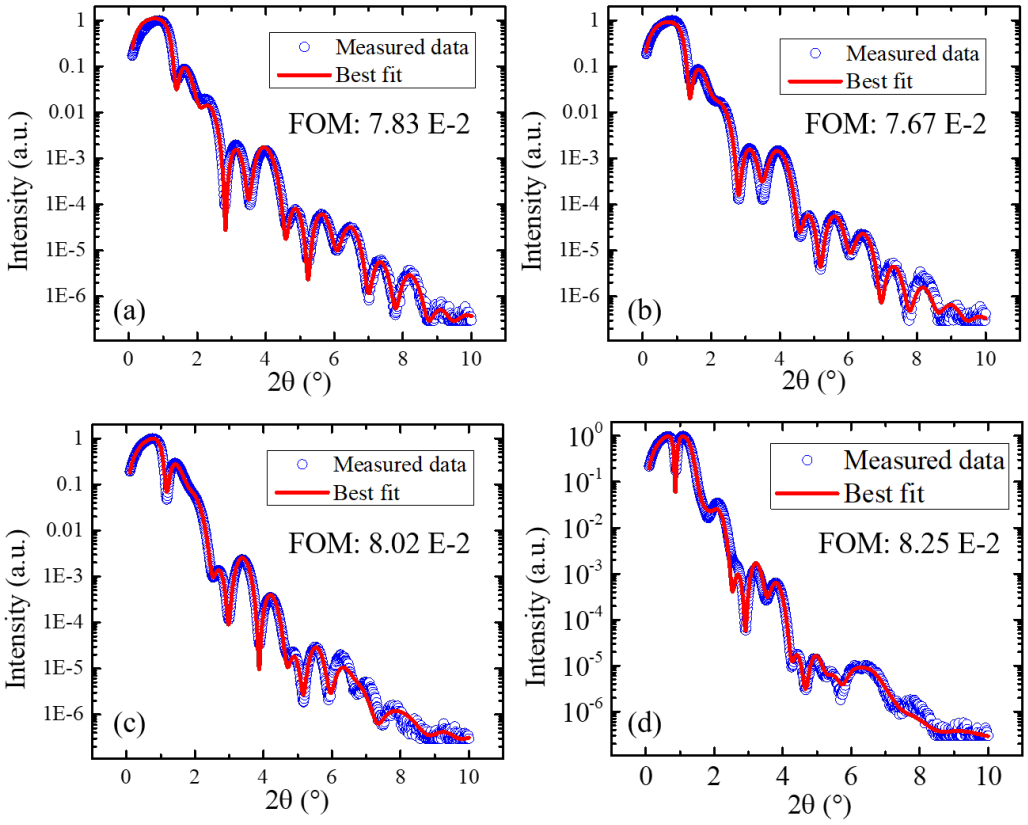

Figure S1: (a-d) XRR data and fitting for sample A1 to A4, respectively considering without any interdiffusion layer. Blue open circles represent measured data and red solid lines are the best fits using GenX software.

Exchange bias measurements:

In such ultrathin films there is a possibility of oxygen penetration which may lead to the formation of CoO. In such scenario the Co/CoO may lead to exchange bias. We have performed exchange bias measurement at 5K at different cooling fields (0 T, +1T and −1T) (Figure S3 (a)). The hysteresis loop did not exhibit any shift under field cooling of ± 1

Table S1: Parameters obtained from XRR fits considering without any interdiffusion layer

	Sample A1		Sample A2		Sample A3		Sample A4	
Layers	t(nm)	σ(nm)	t(nm)	σ(nm)	t(nm)	σ(nm)	t(nm)	σ(nm)
SiO_2 (native oxide)	2.20	0.31	2.30	0.36	2.10	0.39	1.91	0.43
Ta	2.85	0.26	2.91	0.43	3.05	0.35	3.10	0.40
Pt	3.5	0.43	3.31	0.52	3.40	0.49	3.60	0.63
Co	0.79	0.41	0.78	0.42	0.79	0.43	0.81	0.40
C_{60}	-	-	0.48	0.30	1.58	0.65	3.15	0.71
Pt	4.31	0.37	4.29	0.34	4.6	0.35	4.45	0.52

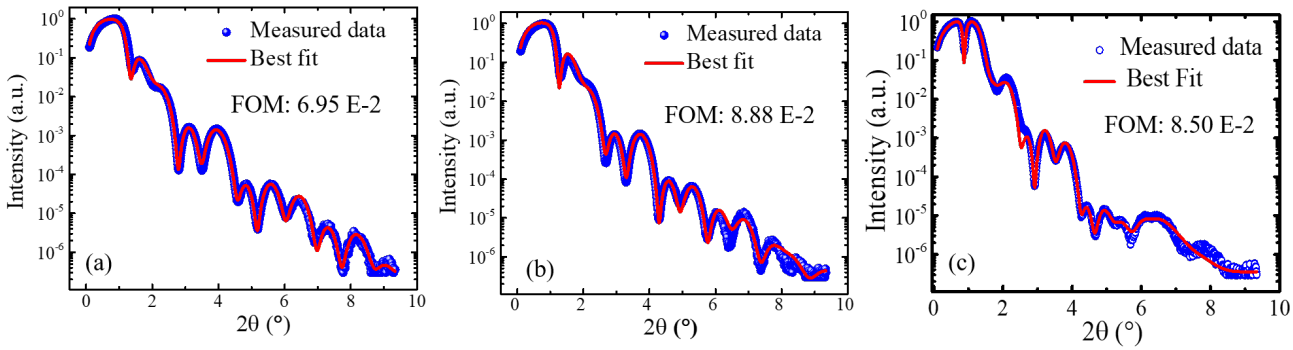

Figure S2: (a-c) XRR data and fitting for sample A2 to A4, respectively considering Pt-C_{60} interdiffusion layer. Blue circles represent measured data and red solid lines are the best fits using GenX software.

Table S2: Parameters obtained from XRR fits considering Pt-C_{60} interdiffusion layer

	Sample A2		Sample A3		Sample A4	
Layers	t(nm)	σ(nm)	t(nm)	σ(nm)	t(nm)	σ(nm)
Ta	2.66	0.35	2.72	0.61	2.67	0.40
Pt	2.98	0.30	2.70	0.99	3.51	0.52
Co	0.72	0.42	0.70	0.48	0.72	0.58
C_{60}	0.30	0.33	0.80	0.72	3.71	1.32
C_{60}-Pt	0.70	0.32	0.73	0.43	1.12	0.78
Pt	3.04	0.36	3.41	0.49	3.7	0.755

Tesla. We have also performed the training effect measurements at 5 K at different cooling field (0.5 T, 1T and 2T) for n= 1 to 4. In this case also we have not observed any loop shift. Figure S3 (b-c) shows the training effect data for sample A3. Therefore, we assume that there is no or very negligible CoO layer is present in our system. In future performing cross sectional TEM will help to understand this.

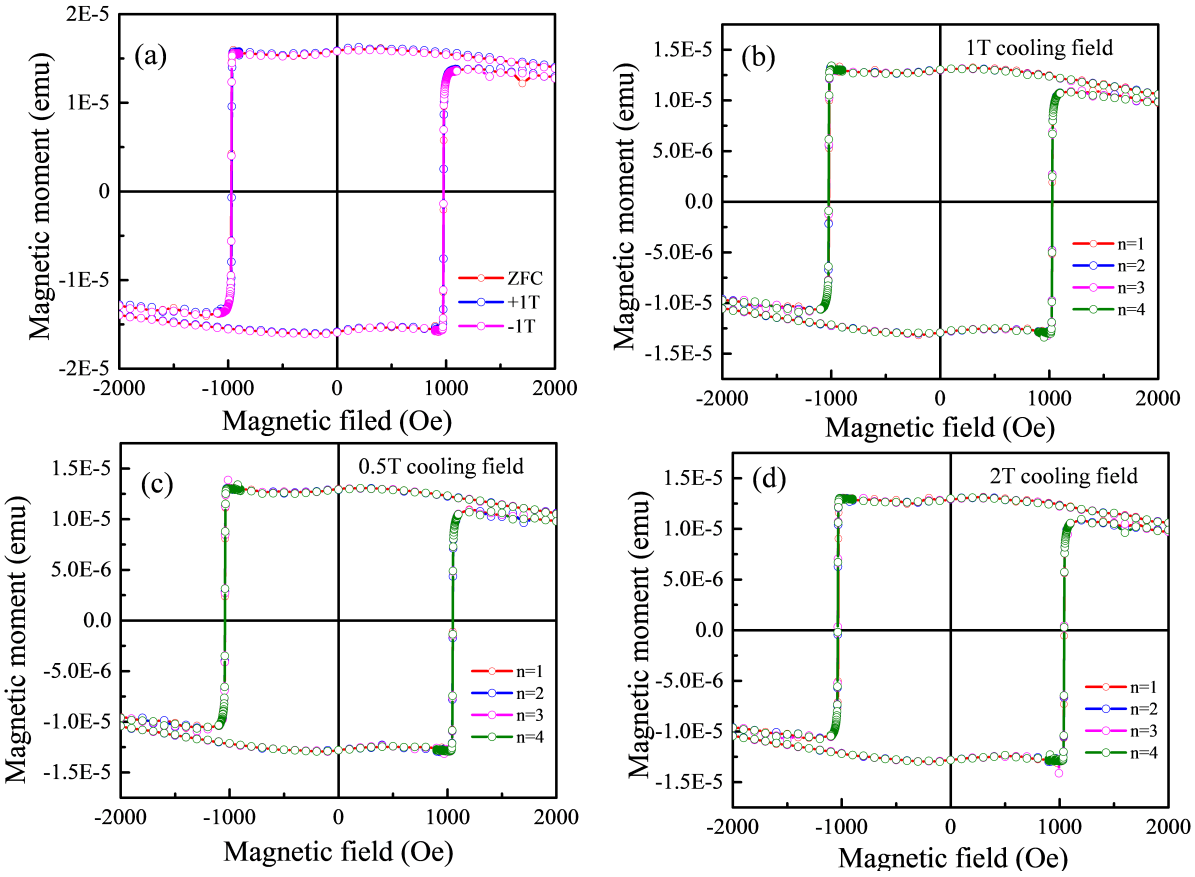

Figure S3: (a) Cooling field dependent hysteresis loops measured at 5K and (b-c) training effect measurement at 5 K at 1T, 0.5T and 2T cooling field for n= 1 to 4, respectively.

Hysteresis loops and domain imaging via Kerr microscopy:

We have prepared Pt/Co/C_{60}/Pt multilayers by varying the C_{60} and Co thickness. The sample structures are the following:

Sample B1: Si/SiO_2 (native oxide)/ Ta (3 nm)/Pt (3.5 nm)/Co (0.6 nm)/Pt (4.5 nm) and

Sample B2: Si/SiO_2 (native oxide)/ Ta (3 nm)/Pt (3.5 nm)/Co (0.6 nm)/C_{60} (0.5 nm)/Pt (4.5 nm)

Sample B3: Si/SiO_2 (native oxide)/ Ta (3 nm)/Pt (3.5 nm)/Co (0.6 nm)/C_{60} (1.6 nm)/Pt (4.5 nm)

Sample B4: Si/SiO_2 (native oxide)/ Ta (3 nm)/Pt (3.5 nm)/Co (0.6 nm)/C_{60} (3.2 nm)/Pt (4.5 nm)

Sample C1: Si/SiO_2 (native oxide)/ Ta (3 nm)/Pt (3.5 nm)/Co (1.0 nm)/Pt (4.5 nm) and

Sample C2: Si/SiO_2 (native oxide)/ Ta (3 nm)/Pt (3.5 nm)/Co (1.0 nm)/C_{60} (1.6 nm)/Pt (4.5 nm)

Sample C3: Si/SiO_2 (native oxide)/ Ta (3 nm)/Pt (3.5 nm)/Co (1.0 nm)/C_{60} (3.2 nm)/Pt (4.5 nm)

For these different series of samples B1-B4 (Co thickness 0.6 nm) and C1-C3 (Co thickness 1 nm), we have also observed coercivity and domain size reduction with increase in C_{60} thickness, which is similar to the main manuscript results. Figure S4 shows the hysteresis loops of all the samples B1-B4 measured by MOKE based microscopy. Figure S5 shows domain images captured at different field points (A-E) marked in hysteresis loops shown in figure S4. Domains are marked in red circles having same diameter (b,g,l,q) and (c,h,m,r). Figure S6 shows the hysteresis loops of all the samples C1-C3 measured by MOKE based microscopy. Figure S7 shows domain images captured at different field points (A-E) marked in hysteresis loops shown in figure S6. Domains are marked in red circles having same diameter (b,g,l), (c,h,m) and (d,i,n).

To check the reproducibility, we have prepared a new series of Pt/Co (0.8nm)/C_{60} ($t_{C_{60}}$)/Pt by varying the thickness ($t_{C_{60}}$) of C_{60} 0 to 50 nm and performed the hysteresis loop measurements and domain imaging. The new series of samples show the similar results like the previous series. Figure S8 shows the hysteresis loops along with domain images for new series. Further we calculated the anisotropy of the samples using SQUID magnetometry. Figure S9 shows the thickness dependence ($t_{C_{60}}$) of effective anisotropy (K_{eff}) (blue solid circles), hard axis saturation field (H_S) (red stars) and saturation magnetization (M_S) (green hexagon). We have observed that anisotropy value is almost constant for the samples

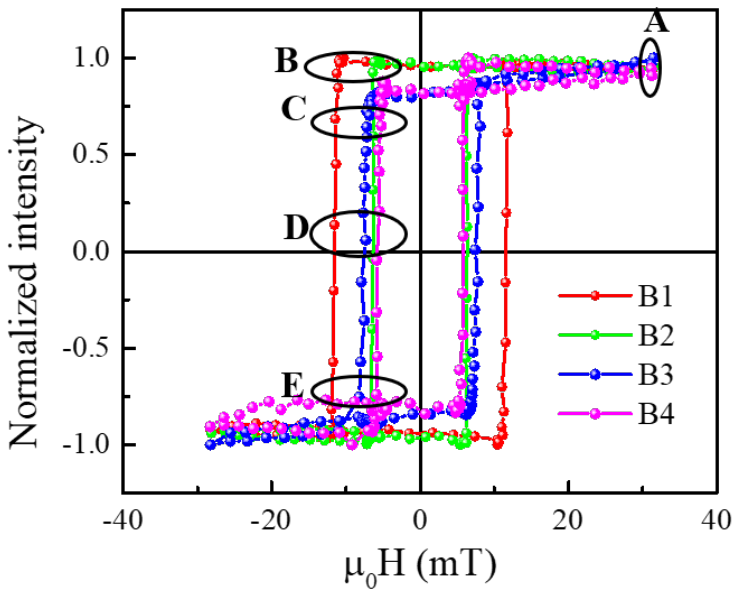

Figure S4: Hysteresis loop measured by MOKE based microscopy in polar mode for samples B1 (red), B2 (green), B3 (blue) and B4 (magenta).

having C_{60} thickness 3.2, 6.4 and 50 nm which shows that the anisotropy enhancing effect saturates after a certain thickness (which is about 2-3 nm in this case).

Distribution of spin moment:

Figures S10 and S11 depict how the spin moments are distributed over different atomic sites at different Co-C_{60} interface. The top layer of the Co slabs is affected mostly by the spinterface formation. There are mainly three types of spin moments at the considered interfaces. These moments have been used to calculate the exchange interactions.

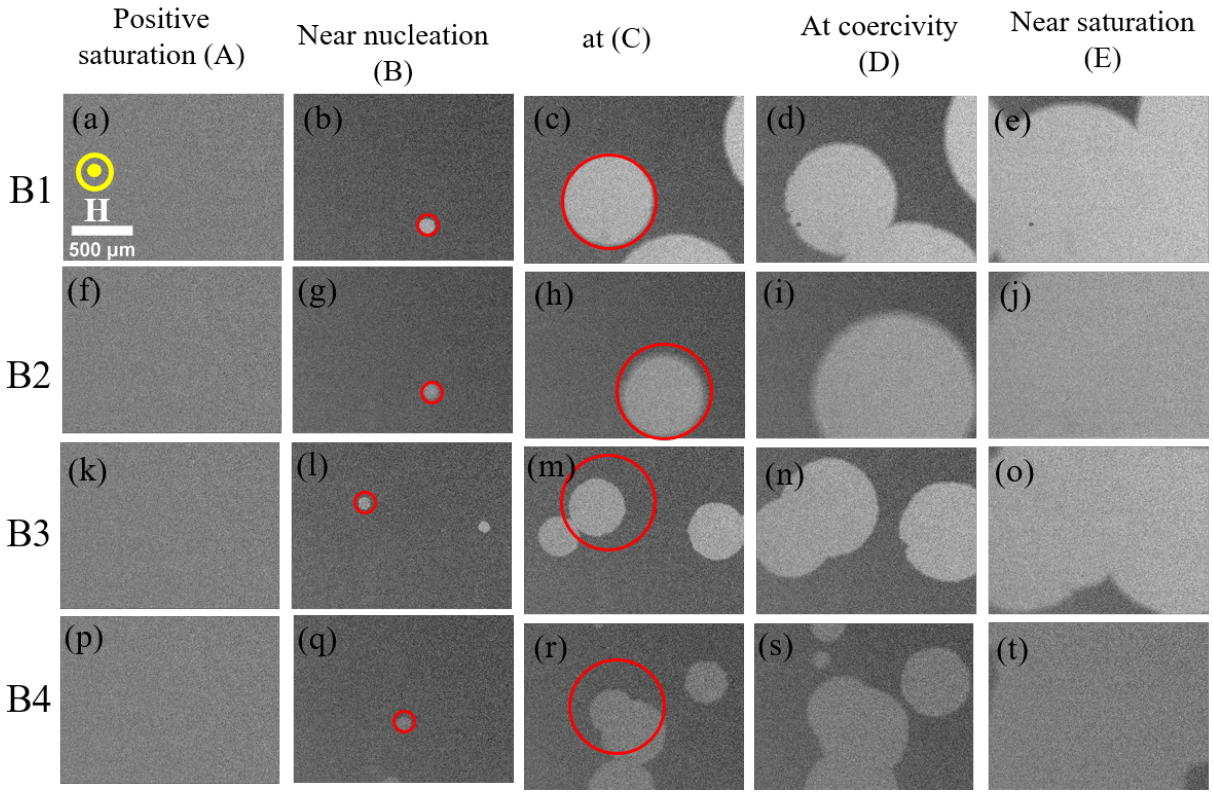

Figure S5: (a-e), (f-j), (k-o) and (p-t) are the domain images for samples B1, B2, B3 and B4, respectively. Domain images are recorded at A-E points of the hysteresis loops shown in figure S4. The direction of the magnetic field and the scale bar is shown (a) and same for all the images.

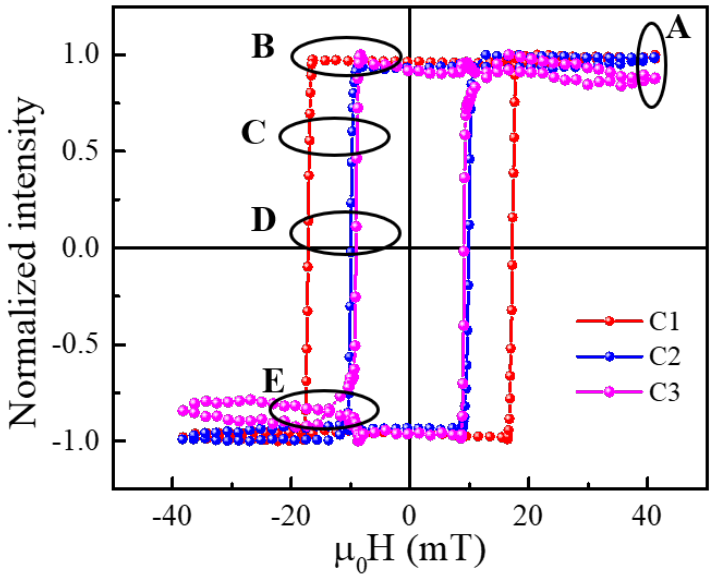

Figure S6: Hysteresis loop measured by MOKE based microscopy in polar mode for samples C1 (red), C2 (blue) and C3 (magenta).

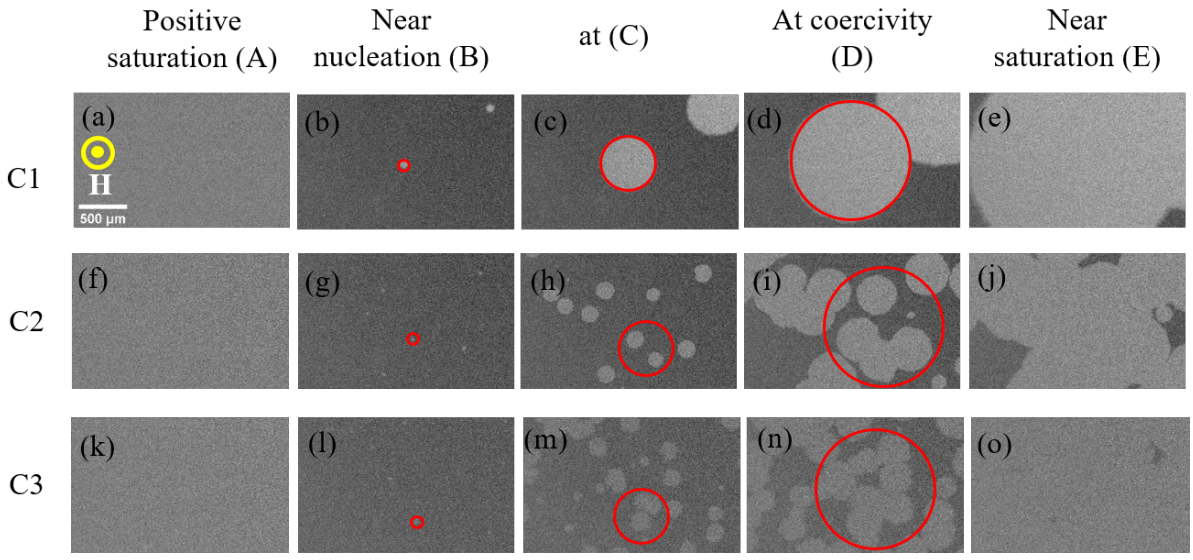

Figure S7: (a-e), (f-j) and (k-o) are the domain images for samples C1, C2 and C3, respectively. Domain images are recorded at A-E points of the hysteresis loops shown in figure S6. The direction of the magnetic field and the scale bar are shown in (a) and same for all the images.

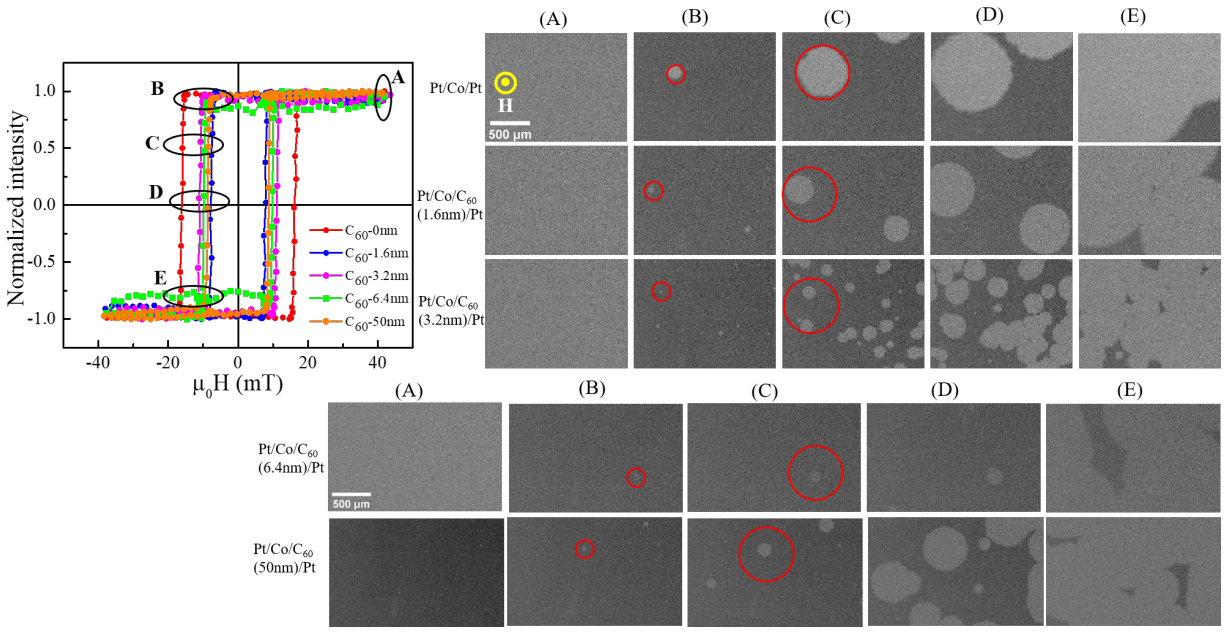

Figure S8: Hysteresis loops and corresponding domain images for the new series of Pt/Co (0.8nm)/C_{60} ($t_{C_{60}}$)/Pt by varying the thickness ($t_{C_{60}}$) of C_{60} 0 to 50 nm. Red circles are used for better visualization and comparing the domain sizes.

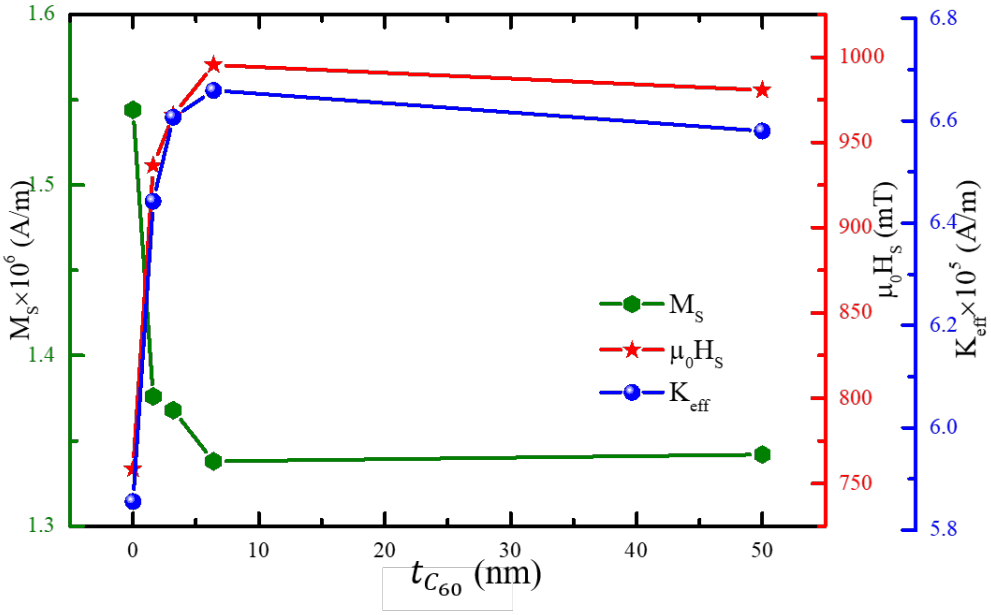

Figure S9: Thickness dependence ($t_{C_{60}}$) of effective anisotropy (K_{eff}) (blue solid circles), hard axis saturation field (H_S) (red stars) and saturation magnetization (M_S) (green hexagon) for Pt/Co (0.8nm)/C_{60}($t_{C_{60}}$)/Pt samples of various $t_{C_{60}}$ thickness.

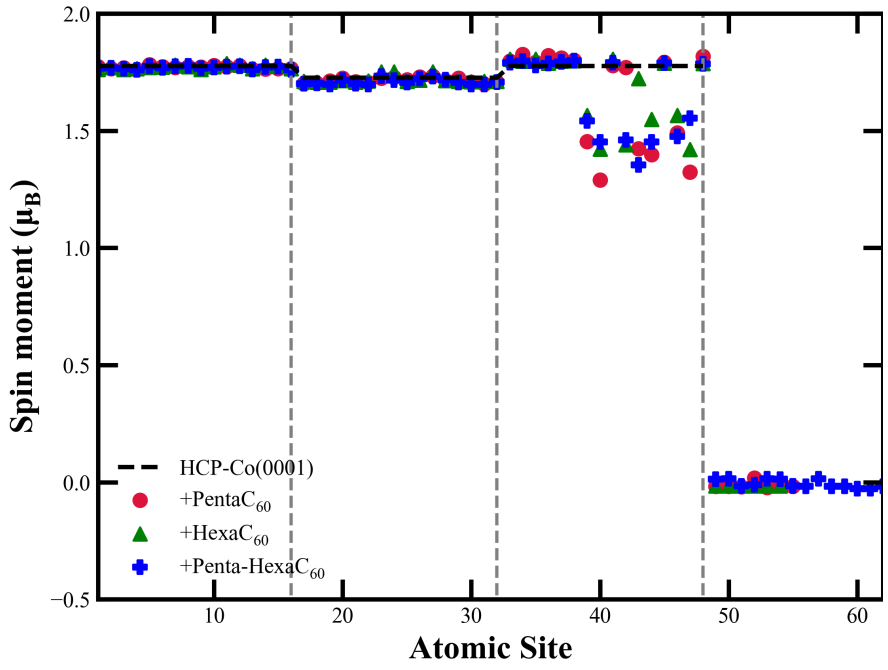

Figure S10: Distribution of spin moments on different atomic sites for HCP-Co (0001) substrate.

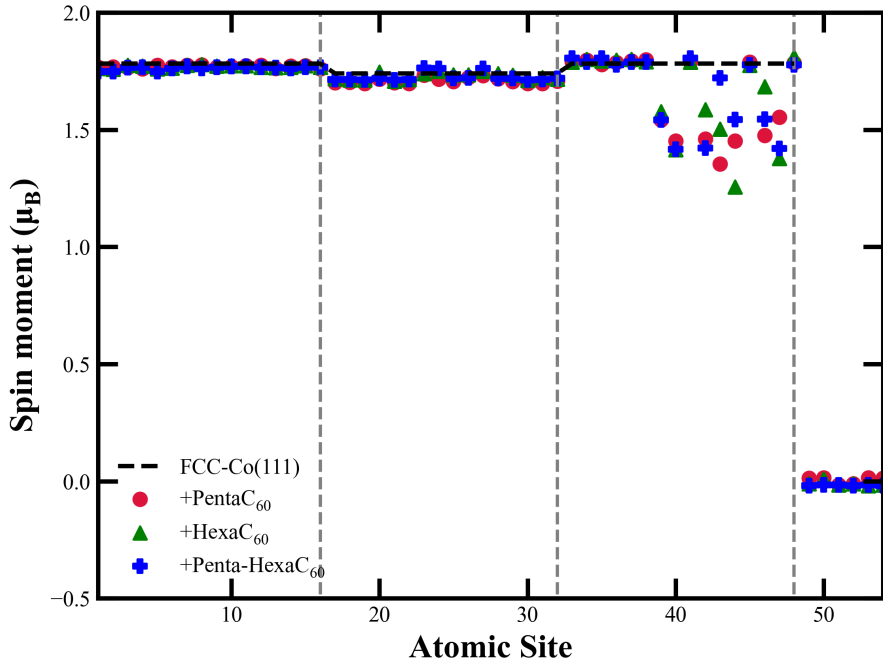

Figure S11: Distribution of spin moments on different atomic sites for FCC-Co (111) substrate.